Journal of Computational and Applied Mathematics 235 (2010) 186–202

Contents lists available at ScienceDirect

Journal of Computational and Applied Mathematics

journal homepage: www.elsevier.com/locate/cam

A posteriori error estimators for nonconforming finite element methods of the linear elasticity problem☆

Kwang-Yeon Kim [a,*], Hyung-Chun Lee [b]

[a] Department of Mathematics, Kangwon National University, Chuncheon 200-701, South Korea

[b] Department of Mathematics, Ajou University, Suwon 443-749, South Korea

ARTICLE INFO

Article history:
Received 29 April 2009
Received in revised form 22 April 2010

MSC:
65N30
65N15

Keywords:
A posteriori error estimators
Nonconforming finite element methods
Linear elasticity problem
Equilibrated residual method

ABSTRACT

In this work we derive and analyze a posteriori error estimators for low-order nonconforming finite element methods of the linear elasticity problem on both triangular and quadrilateral meshes, with hanging nodes allowed for local mesh refinement. First, it is shown that equilibrated Neumann data on interelement boundaries are simply given by the local weak residuals of the numerical solution. The first error estimator is then obtained by applying the equilibrated residual method with this set of Neumann data. From this implicit estimator we also derive two explicit error estimators, one of which is similar to the one proposed by Dörfler and Ainsworth (2005) [24] for the Stokes problem. It is established that all these error estimators are reliable and efficient in a robust way with respect to the Lamé constants. The main advantage of our error estimators is that they yield guaranteed, i.e., constant-free upper bounds for the energy-like error (up to higher order terms due to data oscillation) when a good estimate for the inf–sup constant is available, which is confirmed by some numerical results.

1. Introduction

In this paper we are concerned with a posteriori error analysis for the nonconforming displacement approximation of the linear elasticity equation. It is well known that standard low-order conforming finite elements suffer from so-called *numerical locking*, i.e., the convergence of the numerical solution deteriorates as the material becomes nearly incompressible (cf. [1]). One way to avoid the locking phenomenon is to use the reduced integration of the divergence term. This is closely related to the mixed formulation which introduces the additional "pressure" unknown representing the divergence of the displacement and has the same form as the Stokes problem with the penalty term. Here we are more interested in another common way, that is, nonconforming approximation of the displacement, sometimes combined with the reduced integration technique; see, for example, [1–6].

Nonconforming FEMs typically involve many more unknowns than conforming methods of the same order. Thus it is of practical importance to perform adaptive mesh refinement based on a posteriori error estimators which are expected to provide precise information about the local behavior of the unknown numerical errors. The readers are referred to the books of Ainsworth and Oden [7] and Verfürth [8] for a good survey on various types of a posteriori error estimators and their analysis. There are many works on the study of a posteriori error estimators for the displacement formulation of the linear elasticity problem which are, in addition, desired to be robust in the nearly incompressible regime. Averaging techniques leading to the ZZ estimator are applied in [9,10] for the conforming finite elements and in [11] for the Kouhia–Stenberg

☆ This work was supported by the Korea Research Foundation Grant funded by the Korean Government (KRF-2008-314-C00037).

* Corresponding author.
E-mail addresses: eulerkim@kangwon.ac.kr (K.-Y. Kim), hclee@ajou.ac.kr (H.-C. Lee).

0377-0427/$ – see front matter © 2010 Elsevier B.V. All rights reserved.
doi:10.1016/j.cam.2010.05.032

nonconforming element. Error estimators based on equilibrated fluxes and solution of local Neumann problems are developed in [12–14] for the conforming finite elements, whereas the $\boldsymbol{H}(\mathbf{div})$-conforming approximation of the stress is constructed in [15] to replace the solution of local Neumann problems. For nonconforming FEMs, a unifying framework for residual-based error estimators is given in [16]. We also refer to [17] for a comprehensive review.

The goal of this work is to derive and analyze some implicit and explicit a posteriori error estimators for low-order nonconforming FEMs of the linear elasticity problem on both triangular and quadrilateral meshes, possibly with hanging nodes on their edges (see also a recent work [18] in this direction). Our first step towards this goal is to decompose the numerical *error itself* into two components, *conforming* and *nonconforming* errors (cf. [19–21]). This is mathematically equivalent to the previous approach based on the Helmholtz decomposition of the *gradient of the error* (cf. [16,22–24]) but seems more natural especially in estimating the nonconforming error. To estimate the conforming error, we first introduce an implicit error estimator of the Bank–Weiser type by applying the equilibrated residual method [25,26]. In contrast to [12,13,15,14], where computation of equilibrated fluxes requires quite sophisticated techniques of splitting interelement fluxes obtained by simple averaging, *the equilibrated Neumann data for the edge-based nonconforming elements considered here are simply given by local weak residuals of the numerical solution, even if hanging nodes are present*. Based on these equilibrated fluxes, we also construct the $\boldsymbol{H}(\mathbf{div})$-conforming nonsymmetric tensor field from the lowest-order Raviart–Thomas space, resulting in a ZZ-type explicit error estimator. The same argument was used in [15] for the conforming FEMs on meshes without hanging nodes, but since the symmetric formulation was considered there, the stress approximation was taken to be symmetric, requiring at least cubic finite elements. Furthermore, on triangular and rectangular elements, we can derive an explicit expression for the recovered tensor field in terms of the displacement approximation like in [27], ultimately leading to the simple error estimator which is very similar to the one proposed in [24] for the Stokes problem. Numerical experience indicates that the implicit estimator tends to produce better results but consumes much more time than the explicit ones. The nonconforming error may be estimated by constructing a continuous piecewise polynomial approximation to the (nonconforming) numerical solution (see [19–21] for second-order elliptic problems) which, however, gives rise to severe over-estimation in the nearly incompressible case. The remedy is to employ the continuous inf–sup condition in order to derive a sharper upper bound than the usual one simply based on the energy norm (cf. [24,28]).

It should be mentioned that the results obtained in this work extend those of [24] for the Stokes problem to the linear elasticity problem in several important ways: quadrilateral meshes with hanging nodes are taken into account and an implicit estimator of Bank–Weiser type for the conforming error is defined to improve the explicit estimators. In particular, all error estimators obtained in this work *guarantee constant-free upper bounds* for the true error (up to higher order terms due to data oscillation for the explicit estimators) when a good estimate for the inf–sup constant is available, and are robust with respect to the Lamé constants.

The remainder of the paper is organized as follows. In the next section we introduce some preliminary concepts and notation. Section 3 describes the $P1$ and rotated-$Q1$ nonconforming FEMs for the linear elasticity problem. In Section 4 we discuss how the local Neumann data are computed from the numerical solution and then construct a $\boldsymbol{H}(\mathbf{div})$-conforming tensor field based on those Neumann data. In Section 5 we present a posteriori error estimators and establish their reliability and efficiency. Finally, some numerical experiments are carried out in Section 6 to demonstrate our theoretical results.

2. Preliminaries

Throughout the paper, the vector- and tensor-valued functions will be denoted by boldface letters. For vector-valued functions $\boldsymbol{v} = (v_i)$, $\boldsymbol{w} = (w_i)$ and tensor-valued functions $\boldsymbol{\sigma} = (\sigma_{ij})$, $\boldsymbol{\tau} = (\tau_{ij})$, we define the tensor gradient and the vector divergence by

$$(\nabla \boldsymbol{v})_{ij} = \frac{\partial v_i}{\partial x_j}, \qquad (\mathbf{div}\,\boldsymbol{\tau})_i = \sum_j \frac{\partial \tau_{ij}}{\partial x_j}$$

and the products by

$$\boldsymbol{\sigma} : \boldsymbol{\tau} = \sum_{i,j} \sigma_{ij}\tau_{ij}, \qquad (\boldsymbol{v} \otimes \boldsymbol{w})_{ij} = v_i w_j, \qquad (\boldsymbol{\tau}\boldsymbol{v})_i = \sum_j \tau_{ij} v_j,$$

with $|\boldsymbol{\tau}| = (\boldsymbol{\tau} : \boldsymbol{\tau})^{\frac{1}{2}}$. We adopt the standard notation for the Sobolev spaces and their norms, and set

$$\boldsymbol{H}^1(\Omega) = (H^1(\Omega))^2, \qquad \boldsymbol{H}^1_0(\Omega) = \{\boldsymbol{v} \in \boldsymbol{H}^1(\Omega) : \boldsymbol{v}|_{\partial\Omega} = 0\},$$
$$\boldsymbol{H}(\mathbf{div}\,;\Omega) = \{\boldsymbol{\tau} \in (L^2(\Omega))^{2\times 2} : \mathbf{div}\,\boldsymbol{\tau} \in (L^2(\Omega))^2\}.$$

Let $\mathbb{P}_k(D)$ denote the space of polynomials on D of total degree at most k.

For a bounded domain Ω in $\mathbb{R}^2$ with Lipschitz boundary Γ, we consider the homogeneous isotropic linear elasticity problem with the pure displacement boundary condition described by

$$\begin{cases} -\mathbf{div}\,(2\mu\,\boldsymbol{\epsilon}(\boldsymbol{u}) + \lambda\,\mathrm{div}\,\boldsymbol{u}\boldsymbol{I}) = \boldsymbol{f} & \text{in } \Omega, \\ \boldsymbol{u} = \boldsymbol{u}_D & \text{on } \Gamma, \end{cases} \tag{1}$$

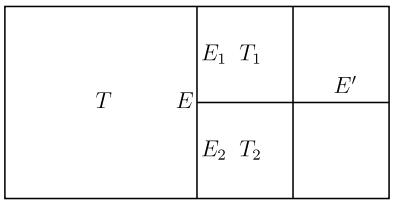

Fig. 1. The edges $E_1 = \partial T \cap \partial T_1$ and $E_2 = \partial T \cap \partial T_2$ are regular but not truly regular. $E = E_1 \cup E_2$ is an irregular edge, and E' is a truly regular edge.

where $\boldsymbol{u}$ is the displacement, $\boldsymbol{\epsilon}(\boldsymbol{v}) = \frac{1}{2}(\nabla \boldsymbol{v} + (\nabla \boldsymbol{v})^t)$ is the strain tensor, $\boldsymbol{I}$ is the 2×2 identity tensor, $\boldsymbol{f} \in (L^2(\Omega))^2$, and $\boldsymbol{u}_D \in (H^{1/2}(\Gamma) \cap C(\Gamma))^2$. An equivalent formulation to problem (1) reads as follows:

$$\begin{cases} -\mu \Delta \boldsymbol{u} - (\lambda + \mu)\nabla(\operatorname{div} \boldsymbol{u}) = \boldsymbol{f} & \text{in } \Omega, \\ \boldsymbol{u} = \boldsymbol{u}_D & \text{on } \Gamma. \end{cases} \tag{2}$$

The standard weak formulation for this problem consists in finding $\boldsymbol{u} \in \boldsymbol{H}^1(\Omega; \boldsymbol{u}_D) := \{\boldsymbol{v} \in \boldsymbol{H}^1(\Omega) : \boldsymbol{v}|_\Gamma = \boldsymbol{u}_D\}$ such that

$$A(\boldsymbol{u}, \boldsymbol{v}) = (\boldsymbol{f}, \boldsymbol{v})_\Omega \quad \forall \boldsymbol{v} \in \boldsymbol{H}_0^1(\Omega),$$

where $(\cdot, \cdot)_\Omega$ is the L^2 inner product over Ω, and

$$A(\boldsymbol{u}, \boldsymbol{v}) = \mu(\nabla \boldsymbol{u}, \nabla \boldsymbol{v})_\Omega + (\lambda + \mu)(\operatorname{div} \boldsymbol{u}, \operatorname{div} \boldsymbol{v})_\Omega.$$

The constants μ and λ are called Lamé constants, and it is assumed that $\mu_1 \le \mu \le \mu_2$ for some $\mu_1, \mu_2 > 0$ and $0 < \lambda < \infty$.

Let $\{\mathcal{T}_h\}_{h>0}$ be a family of regular partitions of Ω into triangles or quadrilaterals, where $h_T := \operatorname{diam}(T)$ and $h := \max_{T \in \mathcal{T}_h} h_T$. When a differential operator is taken piecewise over $\mathcal{T}_h$, this is indicated by the subscript h, like ∇_h and div_h. We allow for hanging nodes on the edges of $\mathcal{T}_h$, but for the sake of simplicity, it is assumed that they are generated by successive refinement of a conforming initial mesh subject to the classical 1-*irregular rule*: *every edge has at most one hanging node on it*. Mesh refinement is performed by refining some elements into smaller sub-elements in such a way that $\mathcal{T}_h$ remains locally quasi-uniform, i.e.,

$$h_T \simeq h_{T'} \simeq h_E := \operatorname{diam}(E)$$

for every nonempty edge $E = \partial T \cap \partial T'$. Later in Section 5.2, we will assume that triangular elements contain no hanging nodes. This can be achieved by further refinement of neighbors (cf. [8]).

We use the notation $\mathcal{E}_T$ and $\boldsymbol{n}_T$ to denote the set of edges of an element $T \in \mathcal{T}_h$ and the unit normal outward to T, respectively. Let $\mathcal{E}_\Gamma$ be the collection of all boundary edges of $\mathcal{T}_h$, and set

$$\mathcal{E}_h = \bigcup_{T \in \mathcal{T}_h} \mathcal{E}_T, \qquad \mathcal{E}_\Omega = \mathcal{E}_h \setminus \mathcal{E}_\Gamma.$$

An edge $E \in \mathcal{E}_\Omega$ is called *regular* if it is the intersection of two adjacent elements, otherwise it is called *irregular*. A regular edge is called *truly regular* if it is not part of an irregular edge. See Fig. 1 for an illustration of these definitions. Note that an irregular edge is a union of two regular edges.

Subsequently, C will denote a generic positive constant which may take different values at different occurrences depending on the geometry of Ω and the shape-regularity of $\mathcal{T}_h$, but is independent of h, μ and λ.

3. Nonconforming FEMs

The Rannacher–Turek space on a quadrilateral T is defined by

$$\mathbb{RQ}_1(T) := \left\{\hat{v} \circ F_T^{-1} : \hat{v} = a + b\hat{x} + c\hat{y} + d(\hat{x}^2 - \hat{y}^2),\ a, b, c, d \in \mathbb{R}\right\},$$

where F_T is the invertible bilinear mapping from $\hat{T} = [0, 1]^2$ onto T. On a general element T, we define the local space

$$\mathbb{NC}(T) = \begin{cases} \mathbb{P}_1(T) & \text{if } T \text{ is a triangle,} \\ \mathbb{RQ}_1(T) & \text{if } T \text{ is a quadrilateral.} \end{cases}$$

It is known that integral averages on the edges of T can be used as degrees of freedom for this space. For each $E \in \mathcal{E}_T$, we denote by $\phi_E^{(T)} \in \mathbb{NC}(T)$ the local basis function such that

$$\int_{E'} \phi_E^{(T)} \, \mathrm{d}s = \delta_{E,E'}|E| \quad \forall E' \in \mathcal{E}_T,$$

where $|D|$ is the measure of a set D.

The nonconforming finite element space on a mesh $\mathcal{T}_h$ is defined by (see [29] for triangular meshes and [30] for quadrilateral meshes)

$$\mathcal{V}_h = \left\{ v_h \in L^2(\Omega) : v_h|_T \in \mathbb{NC}(T)\ \forall T \in \mathcal{T}_h, \text{ and } \int_E [\![v_h]\!]\,\mathrm{d}s = 0\ \forall E \in \mathcal{E}'_\Omega \right\},$$

$$\mathcal{V}_{h,0} = \left\{ v_h \in \mathcal{V}_h : \int_E v_h\,\mathrm{d}s = 0\ \forall E \in \mathcal{E}_\Gamma \right\},$$

where $[\![v]\!]|_E$ is the jump of v across the edge E, and $\mathcal{E}'_\Omega \subset \mathcal{E}_\Omega$ consists of truly regular edges and irregular edges. Observe that the standard weak continuity is imposed on truly regular edges, whereas the matching condition across the irregular edge $E = E_1 \cup E_2$ (see Fig. 1) can be stated as

$$\int_E v_h|_T\,\mathrm{d}s = \int_{E_1} v_h|_{T_1}\,\mathrm{d}s + \int_{E_2} v_h|_{T_2}\,\mathrm{d}s.$$

This implies that *all integral averages on regular edges are counted as independent degrees of freedom*. It is easy to verify that the global basis function ϕ_{E_i} associated with the edge E_i is obtained by patching together the local functions $\phi_E^{(T)}$ and $\phi_{E_i}^{(T_i)}$ in such a way that

$$\phi_{E_i}|_T = \frac{|E_i|}{|E|}\phi_E^{(T)} \quad \text{and} \quad \phi_{E_i}|_{T_i} = \phi_{E_i}^{(T_i)}, \tag{3}$$

with its support in $\overline{T \cup T_i}$.

Let P_h be the L^2 projection onto the space of piecewise constants on $\mathcal{T}_h$, and define the discrete bilinear form (cf. [1,2,5])

$$A_h(\boldsymbol{u}_h, \boldsymbol{v}_h) = \mu(\nabla_h \boldsymbol{u}_h, \nabla_h \boldsymbol{v}_h)_\Omega + (\lambda+\mu)(P_h \operatorname{div}_h \boldsymbol{u}_h, P_h \operatorname{div}_h \boldsymbol{v}_h)_\Omega.$$

Notice that P_h has no effect on triangular elements. Then the nonconforming FEM for problem (2) is to find $\boldsymbol{u}_h \in \mathcal{V}_h \times \mathcal{V}_h$ such that $\int_E (\boldsymbol{u}_h - \boldsymbol{u}_D)\,\mathrm{d}s = 0$ on every $E \in \mathcal{E}_\Gamma$, and

$$A_h(\boldsymbol{u}_h, \boldsymbol{v}_h) = (\boldsymbol{f}, \boldsymbol{v}_h)_\Omega \quad \forall \boldsymbol{v}_h \in \mathcal{V}_{h,0} \times \mathcal{V}_{h,0}. \tag{4}$$

Remark 1. Introduction of the L^2 projection P_h onto the lower-order space, sometimes referred to as the reduced integration of the divergence term, is intended to avoid the numerical locking for large values of λ. This is closely related to the mixed formulation of (2) which introduces the additional "pressure" unknown $p = -(\lambda+\mu)\operatorname{div}\boldsymbol{u}$, leading to the Stokes problem with the penalty term. More examples can be found in [1–3,5,6].

4. Construction of equilibrated fluxes and $H(\mathrm{div})$-conforming tensor field

To apply the equilibrated residual method to the nonconforming FEM (4), we need to construct the normal flux functions $\{\boldsymbol{g}_T \in (L^2(\partial T))^2 : \boldsymbol{g}_T \approx (\mu\nabla\boldsymbol{u} + (\lambda+\mu)\operatorname{div}\boldsymbol{u}\boldsymbol{I})\boldsymbol{n}_T|_{\partial T}\}_{T\in\mathcal{T}_h}$ from the numerical solution $\boldsymbol{u}_h$ such that the following two equilibration conditions are satisfied:

$$\boldsymbol{g}_T + \boldsymbol{g}_{T'} = 0 \quad \text{on } E = \partial T \cap \partial T', \tag{EQ1}$$

$$\int_T \boldsymbol{f}\,\mathrm{d}\boldsymbol{x} + \int_{\partial T} \boldsymbol{g}_T\,\mathrm{d}s = 0 \quad \forall T \in \mathcal{T}_h. \tag{EQ2}$$

To do this, we start with the observation that for a truly regular edge $E = \partial T \cap \partial T'$, the scalar equations obtained by taking $\boldsymbol{v}_h = (\phi_E, 0)^t$ and $(0, \phi_E)^t$ in (4) can be written as a single vector equation

$$\left\{ \int_T (\mu\nabla\boldsymbol{u}_h + (\lambda+\mu)P_h\operatorname{div}\boldsymbol{u}_h\boldsymbol{I})\nabla\phi_E^{(T)}\,\mathrm{d}\boldsymbol{x} - \int_T \boldsymbol{f}\phi_E^{(T)}\,\mathrm{d}\boldsymbol{x} \right\}$$
$$+ \left\{ \int_{T'} (\mu\nabla\boldsymbol{u}_h + (\lambda+\mu)P_h\operatorname{div}\boldsymbol{u}_h\boldsymbol{I})\nabla\phi_E^{(T')}\,\mathrm{d}\boldsymbol{x} - \int_{T'} \boldsymbol{f}\phi_E^{(T')}\,\mathrm{d}\boldsymbol{x} \right\} = 0.$$

Note that the quantity in each curly brace is exactly the local weak residual of the discrete system (4) and was interpreted as the equilibrating nodal force associated with the local basis function $\phi_E^{(T)}$ in [31]. Since there are no corner nodes as the conforming FEMs have, no further resolution of these nodal forces is needed and we can simply define for each $E \in \mathcal{E}_T$

$$\boldsymbol{g}_T|_E = \frac{1}{|E|}\left\{ \int_T (\mu\nabla\boldsymbol{u}_h + (\lambda+\mu)P_h\operatorname{div}\boldsymbol{u}_h\boldsymbol{I})\nabla\phi_E^{(T)}\,\mathrm{d}\boldsymbol{x} - \int_T \boldsymbol{f}\phi_E^{(T)}\,\mathrm{d}\boldsymbol{x} \right\}. \tag{5}$$

This definition leads to

$$\int_{\partial T} \boldsymbol{g}_T\phi_E^{(T)}\,\mathrm{d}s = \int_T (\mu\nabla\boldsymbol{u}_h + (\lambda+\mu)P_h\operatorname{div}\boldsymbol{u}_h\boldsymbol{I})\nabla\phi_E^{(T)}\,\mathrm{d}\boldsymbol{x} - \int_T \boldsymbol{f}\phi_E^{(T)}\,\mathrm{d}\boldsymbol{x}$$

which is an equivalent form of the prolongation condition of Ladevèze (cf. [31]).

Theorem 1. *The piecewise constant functions $\{\boldsymbol{g}_T\}_{T\in\mathcal{T}_h}$ defined by (5) fulfill the equilibration conditions (EQ1)–(EQ2).*

Proof. The first condition (EQ1) is obvious on truly regular edges by construction. On an irregular edge $E \in \mathcal{E}_T$ as shown in Fig. 1, we take $\boldsymbol{v}_h = (\phi_{E_i}, 0)^t$ and $(0, \phi_{E_i})^t$ in (4) and then use (3) to obtain

$$\frac{|E_i|}{|E|}\left\{\int_T (\mu\nabla\boldsymbol{u}_h + (\lambda+\mu)P_h \operatorname{div}\boldsymbol{u}_h\boldsymbol{I})\nabla\phi_E^{(T)}\,\mathrm{d}\boldsymbol{x} - \int_T \boldsymbol{f}\phi_E^{(T)}\,\mathrm{d}\boldsymbol{x}\right\} + \left\{\int_{T_i} (\mu\nabla\boldsymbol{u}_h + (\lambda+\mu)P_h \operatorname{div}\boldsymbol{u}_h\boldsymbol{I})\nabla\phi_{E_i}^{(T_i)}\,\mathrm{d}\boldsymbol{x} - \int_{T_i} \boldsymbol{f}\phi_{E_i}^{(T_i)}\,\mathrm{d}\boldsymbol{x}\right\} = 0,$$

which immediately gives

$$\boldsymbol{g}_T|_E + \boldsymbol{g}_{T_i}|_{E_i} = 0 \quad i = 1, 2.$$

This proves (EQ1) for all regular edges.

The second condition (EQ2) follows directly from the equality

$$\int_{\partial T} \boldsymbol{g}_T\,\mathrm{ds} = \sum_{E\in\mathcal{E}_T}\left\{\int_T (\mu\nabla\boldsymbol{u}_h + (\lambda+\mu)P_h \operatorname{div}\boldsymbol{u}_h\boldsymbol{I})\nabla\phi_E^{(T)}\,\mathrm{d}\boldsymbol{x} - \int_T \boldsymbol{f}\phi_E^{(T)}\,\mathrm{d}\boldsymbol{x}\right\}$$

since $\sum_{E\in\mathcal{E}_T}\phi_E^{(T)} \equiv 1$ on T. □

To recover a tensor field from the normal flux function $\boldsymbol{g}_T$, we define the lowest order Raviart–Thomas space (cf. [32])

$$\mathbb{RT}_0(T) := \{\boldsymbol{v} : \boldsymbol{v} = (a + bx, c + by),\ a, b, c \in \mathbb{R}\}$$

if T is a triangle, and

$$\mathbb{RT}_0(T) := \{\boldsymbol{v} : \boldsymbol{v} = (a + bx, c + \mathrm{d}y), a, b, c, d \in \mathbb{R}\}$$

if T is a rectangle. On a general quadrilateral T, it can be defined via the Piola transformation

$$\mathbb{RT}_0(T) := \{\boldsymbol{v} : \boldsymbol{v} = (\det DF_T)^{-1} DF_T\hat{\boldsymbol{v}}, \hat{\boldsymbol{v}} \in \mathbb{RT}_0(\hat{T})\},$$

where DF_T is the Jacobian matrix of F_T. The product $\mathbb{RT}_0(T) \times \mathbb{RT}_0(T)$ will denote the space of all tensor-valued functions whose rows belong to $\mathbb{RT}_0(T)$.

It is well known that $\boldsymbol{v} \in \mathbb{RT}_0(T)$ has constant normal components on the edges of T which can be used as degrees of freedom for $\mathbb{RT}_0(T)$. The local basis function $\boldsymbol{\theta}_E^{(T)} \in \mathbb{RT}_0(T)$ associated with the edge $E \in \mathcal{E}_T$ is defined by

$$\int_{E'} \boldsymbol{\theta}_E^{(T)} \cdot \boldsymbol{n}_T\,\mathrm{ds} = |E'|\,\boldsymbol{\theta}_E^{(T)} \cdot \boldsymbol{n}_T|_{E'} = \delta_{E,E'} \quad \forall E' \in \mathcal{E}_T.$$

Then the following identity holds true for all $\boldsymbol{\tau} \in \mathbb{RT}_0(T) \times \mathbb{RT}_0(T)$:

$$\boldsymbol{\tau} = \sum_{E\in\mathcal{E}_T}\left(\int_E \boldsymbol{\tau}\boldsymbol{n}_T\,\mathrm{ds}\right) \otimes \boldsymbol{\theta}_E^{(T)} = \sum_{E\in\mathcal{E}_T} |E|\,\boldsymbol{\tau}\boldsymbol{n}_T|_E \otimes \boldsymbol{\theta}_E^{(T)}. \tag{6}$$

On each $T \in \mathcal{T}_h$, we now construct the nonsymmetric tensor field $\boldsymbol{\sigma}_h|_T$ such that $\boldsymbol{\sigma}_h|_T\boldsymbol{n}_T = \boldsymbol{g}_T$, with $\boldsymbol{g}_T$ given by (5). Since $\boldsymbol{g}_T$ is constant on each edge of T, it is natural to seek $\boldsymbol{\sigma}_h|_T$ in $\mathbb{RT}_0(T) \times \mathbb{RT}_0(T)$ and define it by

$$\boldsymbol{\sigma}_h|_T = \sum_{E\in\mathcal{E}_T} |E|\,\boldsymbol{g}_T|_E \otimes \boldsymbol{\theta}_E^{(T)} \quad \forall T \in \mathcal{T}_h. \tag{7}$$

By the continuity condition (EQ1), it is ensured that $\boldsymbol{\sigma}_h$ has continuous normal components across interior edges of $\mathcal{T}_h$, and thus $\boldsymbol{\sigma}_h \in \boldsymbol{H}(\mathbf{div}; \Omega)$. The following theorem states some crucial properties of $\boldsymbol{\sigma}_h$ which will be used in deriving explicit error estimators in the subsequent section.

Theorem 2. *Let $\boldsymbol{\sigma}_h$ be defined by (7), and define $Q_h\boldsymbol{f}$ by*

$$Q_h\boldsymbol{f}|_T = \begin{cases} P_h\boldsymbol{f}|_T & \text{if } T \text{ is a triangle,} \\ \dfrac{1}{\det DF_T}\displaystyle\int_T \boldsymbol{f}\,\mathrm{d}\boldsymbol{x} & \text{if } T \text{ is a quadrilateral.} \end{cases}$$

Then we have

$$\int_T (\mathbf{div}\,\boldsymbol{\sigma}_h + \boldsymbol{f})\,\mathrm{d}\boldsymbol{x} = 0 \quad \textit{and} \quad \mathbf{div}\,\boldsymbol{\sigma}_h + Q_h\boldsymbol{f} = 0. \tag{8}$$

Moreover, $\boldsymbol{\sigma}_h$ has the following explicit formula

$$\boldsymbol{\sigma}_h|_T = (\mu\nabla\boldsymbol{u}_h + (\lambda+\mu)P_h \operatorname{div}\boldsymbol{u}_h\boldsymbol{I})|_T - \sum_{E\in\mathcal{E}_T}\left(\int_T (\boldsymbol{f}+\mu\Delta\boldsymbol{u}_h)\phi_E^{(T)}\,\mathrm{d}\boldsymbol{x}\right)\otimes\boldsymbol{\theta}_E^{(T)}, \tag{9}$$

if T is a triangle or a rectangle.

Proof. The first equality of (8) is a direct consequence of (EQ2), and the second equality of (8) follows easily from it if T is a triangle, since $\mathbf{div}\,\boldsymbol{\sigma}_h|_T$ is constant. For a quadrilateral T, one can verify that for all $\boldsymbol{v}\in\mathbb{RT}_0(T)$,

$$\operatorname{div}\boldsymbol{v} = \frac{1}{\det DF_T}\int_T \operatorname{div}\boldsymbol{v}\,\mathrm{d}\boldsymbol{x}.$$

Hence, using integration by parts and (EQ2), we obtain

$$\mathbf{div}\,\boldsymbol{\sigma}_h|_T = \frac{1}{\det DF_T}\int_{\partial T}\boldsymbol{\sigma}_h\boldsymbol{n}_T\,\mathrm{d}s = \frac{1}{\det DF_T}\int_{\partial T}\boldsymbol{g}_T\,\mathrm{d}s = -\frac{1}{\det DF_T}\int_T\boldsymbol{f}\,\mathrm{d}\boldsymbol{x},$$

which is nothing but (8).

Now we prove (9) for a triangle or a rectangle T. First note that

$$(\mu\nabla\boldsymbol{u}_h + (\lambda+\mu)P_h\operatorname{div}\boldsymbol{u}_h\boldsymbol{I})|_T \in \mathbb{RT}_0(T)\times\mathbb{RT}_0(T),$$

and thus $(\mu\nabla\boldsymbol{u}_h + (\lambda+\mu)P_h\operatorname{div}\boldsymbol{u}_h\boldsymbol{I})|_T\boldsymbol{n}_T$ is constant on each edge of T. Consequently, it follows that

$$\begin{aligned}\boldsymbol{g}_T|_E &= \frac{1}{|E|}\left\{\int_{\partial T}(\mu\nabla\boldsymbol{u}_h + (\lambda+\mu)P_h\operatorname{div}\boldsymbol{u}_h\boldsymbol{I})\boldsymbol{n}_T\phi_E^{(T)}\,\mathrm{d}\boldsymbol{x} - \int_T(\boldsymbol{f}+\mu\Delta\boldsymbol{u}_h)\phi_E^{(T)}\,\mathrm{d}\boldsymbol{x}\right\}\\ &= (\mu\nabla\boldsymbol{u}_h + (\lambda+\mu)P_h\operatorname{div}\boldsymbol{u}_h\boldsymbol{I})|_T\boldsymbol{n}_T|_E - \frac{1}{|E|}\int_T(\boldsymbol{f}+\mu\Delta\boldsymbol{u}_h)\phi_E^{(T)}\,\mathrm{d}\boldsymbol{x}.\end{aligned}$$

The formula (9) is then obtained by inserting

$$(\boldsymbol{\sigma}_h - \mu\nabla\boldsymbol{u}_h - (\lambda+\mu)P_h\operatorname{div}\boldsymbol{u}_h\boldsymbol{I})|_T\boldsymbol{n}_T|_E = -\frac{1}{|E|}\int_T(\boldsymbol{f}+\mu\Delta\boldsymbol{u}_h)\phi_E^{(T)}\,\mathrm{d}\boldsymbol{x}$$

into the identity (6). □

Remark 2. If $\boldsymbol{f}|_T$ is constant, then (9) can be further simplified to

$$\boldsymbol{\sigma}_h|_T = (\mu\nabla\boldsymbol{u}_h + (\lambda+\mu)P_h\operatorname{div}\boldsymbol{u}_h\boldsymbol{I})|_T - \frac{1}{2}(\boldsymbol{f}+\mu\Delta\boldsymbol{u}_h)|_T\otimes(\boldsymbol{x}-\boldsymbol{x}_T),$$

where $\boldsymbol{x}_T$ is the centroid of T, and we used the identity

$$\sum_{E\in\mathcal{E}_T}\boldsymbol{\theta}_E^{(T)} = \frac{\operatorname{card}(\mathcal{E}_T)}{2|T|}(\boldsymbol{x}-\boldsymbol{x}_T).$$

5. A posteriori error estimators

In this section we derive and analyze some a posteriori error estimators for the nonconforming FEM (4). Our starting point towards this end is to decompose the discretization error into two components, namely, *conforming* and *nonconforming* errors; see [19–21].

We define $\boldsymbol{\xi}\in\boldsymbol{H}^1(\Omega;\boldsymbol{u}_D)$ as the "projection" of $\boldsymbol{u}_h$ onto the solution space $\boldsymbol{H}^1(\Omega;\boldsymbol{u}_D)$ with respect to the energy inner product:

$$A(\boldsymbol{\xi},\boldsymbol{v}) = A_h(\boldsymbol{u}_h,\boldsymbol{v}) \quad \forall\boldsymbol{v}\in\boldsymbol{H}_0^1(\Omega) \tag{10}$$

subject to the Dirichlet boundary condition $\boldsymbol{\xi}|_\Gamma = \boldsymbol{u}_D$. We then decompose the total error into two components

$$\boldsymbol{u}-\boldsymbol{u}_h = (\boldsymbol{u}-\boldsymbol{\xi}) + (\boldsymbol{\xi}-\boldsymbol{u}_h),$$

and estimate each component independently of the other one.

The continuous energy norm $|||\cdot||| := A(\cdot,\cdot)^{1/2}$ is not appropriate for estimating errors on quadrilateral elements, as $|||\boldsymbol{u}-\boldsymbol{u}_h|||$ does not converge to zero uniformly in λ. Instead, the discrete energy norm $|||\cdot|||_h := A_h(\cdot,\cdot)^{1/2}$ was used in [5] for a priori error analysis. Here we adopt the following energy-like error between $\boldsymbol{v}\in\boldsymbol{H}^1(\Omega)$ and $\boldsymbol{u}_h$

$$E_h(\boldsymbol{v},\boldsymbol{u}_h) := \left(\mu\|\nabla_h(\boldsymbol{v}-\boldsymbol{u}_h)\|_{0,\Omega}^2 + (\lambda+\mu)\|\operatorname{div}\boldsymbol{v} - P_h\operatorname{div}_h\boldsymbol{u}_h\|_{0,\Omega}^2\right)^{1/2}$$

which may be viewed as intermediate between $|||\boldsymbol{v}-\boldsymbol{u}_h|||$ and $|||\boldsymbol{v}-\boldsymbol{u}_h|||_h$. Note that the three errors are identical on triangular meshes. Moreover, the following Pythagorean equality holds true

$$E_h(\boldsymbol{u},\boldsymbol{u}_h)^2 = |||\boldsymbol{u}-\boldsymbol{\xi}|||^2 + E_h(\boldsymbol{\xi},\boldsymbol{u}_h)^2$$

which follows readily from the Galerkin orthogonality obtained by taking $\boldsymbol{v}=\boldsymbol{u}-\boldsymbol{\xi}$ in (10).

Remark 3. One may deal with the mixed formulation of (2) by introducing the continuous and discrete pressure variables

$$p=-(\lambda+\mu)\operatorname{div}\boldsymbol{u}, \qquad p_h=-(\lambda+\mu)P_h\operatorname{div}_h\boldsymbol{u}_h.$$

Then $E_h(\boldsymbol{u},\boldsymbol{u}_h)$ can be written in the form of a norm

$$E_h(\boldsymbol{u},\boldsymbol{u}_h)=\left(\mu\|\nabla_h(\boldsymbol{u}-\boldsymbol{u}_h)\|_{0,\Omega}^2+\frac{1}{\lambda+\mu}\|p-p_h\|_{0,\Omega}^2\right)^{1/2}.$$

See [28] for the residual-type estimators of the mixed formulation.

We will refer to $|||\boldsymbol{u}-\boldsymbol{\xi}|||$ and $E_h(\boldsymbol{\xi},\boldsymbol{u}_h)$ as the *conforming* and *nonconforming errors*, respectively. The following lemma provides an abstract upper bound for each component.

Lemma 3. *Define the residual functional* $\mathcal{R}_h:\boldsymbol{H}_0^1(\Omega)\to\mathbb{R}$ *by*

$$\mathcal{R}_h(\boldsymbol{v}):=(\boldsymbol{f},\boldsymbol{v})_\Omega-A_h(\boldsymbol{u}_h,\boldsymbol{v}),$$

and let $m>0$ *be the inf–sup constant from*

$$\sup_{\boldsymbol{v}\in\boldsymbol{H}_0^1(\Omega)}\frac{(\operatorname{div}\boldsymbol{v},q)}{\|\nabla\boldsymbol{v}\|_{0,\Omega}}\geq m\|q\|_{0,\Omega}\quad\forall q\in L_0^2(\Omega). \tag{11}$$

Then we have

$$|||\boldsymbol{u}-\boldsymbol{\xi}|||=\sup_{\boldsymbol{v}\in\boldsymbol{H}_0^1(\Omega)}\frac{\mathcal{R}_h(\boldsymbol{v})}{|||\boldsymbol{v}|||} \tag{12}$$

and

$$E_h(\boldsymbol{\xi},\boldsymbol{u}_h)\leq\inf_{\boldsymbol{\chi}\in\boldsymbol{H}^1(\Omega;\boldsymbol{u}_D)}\mu^{1/2}\left(\|\nabla_h(\boldsymbol{\chi}-\boldsymbol{u}_h)\|_{0,\Omega}+\frac{1}{m}\|\operatorname{div}\boldsymbol{\chi}-P_h\operatorname{div}_h\boldsymbol{u}_h\|_{0,\Omega}\right). \tag{13}$$

Proof. We start with the error equation for $\boldsymbol{v}\in\boldsymbol{H}_0^1(\Omega)$

$$A(\boldsymbol{u}-\boldsymbol{\xi},\boldsymbol{v})=(\boldsymbol{f},\boldsymbol{v})_\Omega-A_h(\boldsymbol{u}_h,\boldsymbol{v})=\mathcal{R}_h(\boldsymbol{v}).$$

Setting $\boldsymbol{v}=\boldsymbol{u}-\boldsymbol{\xi}$, it follows that

$$|||\boldsymbol{u}-\boldsymbol{\xi}|||^2=\mathcal{R}_h(\boldsymbol{u}-\boldsymbol{\xi})\leq\left(\sup_{\boldsymbol{v}\in\boldsymbol{H}_0^1(\Omega)}\frac{\mathcal{R}_h(\boldsymbol{v})}{|||\boldsymbol{v}|||}\right)|||\boldsymbol{u}-\boldsymbol{\xi}|||,$$

which proves (12). To derive (13), let $\boldsymbol{\chi}$ be an arbitrary function in $\boldsymbol{H}^1(\Omega;\boldsymbol{u}_D)$. Taking $\boldsymbol{v}=\boldsymbol{\xi}-\boldsymbol{\chi}$ in (10), we obtain

$$\begin{aligned}E_h(\boldsymbol{\xi},\boldsymbol{u}_h)^2 &= \mu(\nabla_h(\boldsymbol{\xi}-\boldsymbol{u}_h),\nabla_h(\boldsymbol{\chi}-\boldsymbol{u}_h))+(\lambda+\mu)(\operatorname{div}\boldsymbol{\xi}-P_h\operatorname{div}_h\boldsymbol{u}_h,\operatorname{div}\boldsymbol{\chi}-P_h\operatorname{div}_h\boldsymbol{u}_h)\\ &\leq \mu\|\nabla_h(\boldsymbol{\xi}-\boldsymbol{u}_h)\|_{0,\Omega}\|\nabla_h(\boldsymbol{\chi}-\boldsymbol{u}_h)\|_{0,\Omega}+(\lambda+\mu)\|\operatorname{div}\boldsymbol{\xi}-P_h\operatorname{div}_h\boldsymbol{u}_h\|_{0,\Omega}\|\operatorname{div}\boldsymbol{\chi}-P_h\operatorname{div}_h\boldsymbol{u}_h\|_{0,\Omega}.\end{aligned}$$

On the other hand, noting that

$$\int_\Omega(\operatorname{div}\boldsymbol{\xi}-P_h\operatorname{div}_h\boldsymbol{u}_h)\,d\boldsymbol{x}=\sum_{T\in\mathcal{T}_h}\int_{\partial T}(\boldsymbol{\xi}-\boldsymbol{u}_h)\cdot\boldsymbol{n}_T\,ds=\int_\Gamma(\boldsymbol{u}_D-\boldsymbol{u}_h)\cdot\boldsymbol{n}\,ds=0,$$

one can deduce from (10) and the inf–sup condition (11) that

$$\begin{aligned}(\lambda+\mu)\|\operatorname{div}\boldsymbol{\xi}-P_h\operatorname{div}_h\boldsymbol{u}_h\|_{0,\Omega} &\leq \frac{1}{m}\sup_{\boldsymbol{v}\in\boldsymbol{H}_0^1(\Omega)}\frac{(\lambda+\mu)(\operatorname{div}\boldsymbol{\xi}-P_h\operatorname{div}_h\boldsymbol{u}_h,\operatorname{div}\boldsymbol{v})_\Omega}{\|\nabla\boldsymbol{v}\|_{0,\Omega}}\\ &= \frac{1}{m}\sup_{\boldsymbol{v}\in\boldsymbol{H}_0^1(\Omega)}\frac{-\mu(\nabla_h(\boldsymbol{\xi}-\boldsymbol{u}_h),\nabla\boldsymbol{v})_\Omega}{\|\nabla\boldsymbol{v}\|_{0,\Omega}}\\ &\leq \frac{\mu}{m}\|\nabla_h(\boldsymbol{\xi}-\boldsymbol{u}_h)\|_{0,\Omega},\end{aligned}$$

which yields

$$E_h(\boldsymbol{\xi}, \boldsymbol{u}_h) \le \mu^{1/2} \left(\|\nabla_h(\boldsymbol{\chi} - \boldsymbol{u}_h)\|_{0,\Omega} + \frac{1}{m} \| \operatorname{div} \boldsymbol{\chi} - P_h \operatorname{div}_h \boldsymbol{u}_h \|_{0,\Omega} \right).$$

The proof is completed by taking the infimum over $\boldsymbol{\chi} \in \boldsymbol{H}^1(\Omega; \boldsymbol{u}_D)$. □

5.1. Conforming error estimator

We apply the equilibrated residual method to derive an upper bound for the right-hand side of (12). Let $A_T(\cdot,\cdot)$ and $A_{h,T}(\cdot,\cdot)$ represent the local contributions of $A(\cdot,\cdot)$ and $A_h(\cdot,\cdot)$, respectively, that is,

$$A(\cdot,\cdot) = \sum_{T\in\mathcal{T}_h} A_T(\cdot,\cdot), \qquad A_h(\cdot,\cdot) = \sum_{T\in\mathcal{T}_h} A_{h,T}(\cdot,\cdot).$$

Local Neumann problem. Find $\boldsymbol{\psi}_T \in \boldsymbol{H}^1(T)$ such that for all $\boldsymbol{v} \in \boldsymbol{H}^1(T)$,

$$A_T(\boldsymbol{\psi}_T, \boldsymbol{v}) = (\boldsymbol{f}, \boldsymbol{v})_T + \langle \boldsymbol{g}_T, \boldsymbol{v} \rangle_{\partial T} - A_{h,T}(\boldsymbol{u}_h, \boldsymbol{v}), \tag{14}$$

with the Neumann datum $\boldsymbol{g}_T$ given by (5). The conforming error estimator is then defined as

$$\eta_C := \left(\sum_{T\in\mathcal{T}_h} |\!|\!| \boldsymbol{\psi}_T |\!|\!|_T^2 \right)^{1/2} \quad \text{where } |\!|\!| \boldsymbol{\psi}_T |\!|\!|_T^2 := A_T(\boldsymbol{\psi}_T, \boldsymbol{\psi}_T). \tag{15}$$

Remark 4. Thanks to the condition (EQ2), the problem (14) admits a unique solution up to an additive constant which will not affect subsequent results. In practical computations, these local Neumann problems are solved in finite-dimensional spaces, for example, $(\mathbb{P}_k(T))^2$ for large enough k.

From the *implicit* estimator η_C we will derive the following *explicit* estimator based on the recovered tensor field $\boldsymbol{\sigma}_h$

$$\eta_{SR,T} := \mu^{-1/2} \|\boldsymbol{\sigma}_h - \mu \nabla \boldsymbol{u}_h - (\lambda+\mu) P_h \operatorname{div} \boldsymbol{u}_h \boldsymbol{I}\|_{0,T}.$$

For a triangle or a rectangle T, we can further derive

$$\eta_{\mathrm{DA},T} := \mu^{-1/2} \left\| \frac{1}{2} (P_h \boldsymbol{f} + \mu \Delta \boldsymbol{u}_h) \otimes (\boldsymbol{x} - \boldsymbol{x}_T) \right\|_{0,T}$$

which was originally proposed for the $P1$ nonconforming FEM of the Stokes problem [24]. The corresponding global estimators are denoted by $\eta_{\mathrm{SR}} = \left(\sum_{T\in\mathcal{T}_h} \eta_{SR,T}^2 \right)^{1/2}$ and $\eta_{\mathrm{DA}} = \left(\sum_{T\in\mathcal{T}_h} \eta_{\mathrm{DA},T}^2 \right)^{1/2}$.

The following theorem establishes the reliability of all error estimators defined above, stating that they are guaranteed upper bounds for the conforming error, up to a higher order term for piecewise smooth $\boldsymbol{f}$ in the case of the explicit estimators.

Theorem 4. *We have*

$$|\!|\!| \boldsymbol{u} - \boldsymbol{\xi} |\!|\!| \le \eta_C \le \eta_{\mathrm{SR}} + C\mu^{-1/2} \operatorname{osc}(\boldsymbol{f}, \mathcal{T}_h),$$

where the extra term $\operatorname{osc}(\boldsymbol{f}, \mathcal{T}_h)$ *is the data oscillation of* $\boldsymbol{f}$ *defined by*

$$\operatorname{osc}(\boldsymbol{f}, \mathcal{T}_h) := \left(\sum_{T\in\mathcal{T}_h} h_T^2 \|\boldsymbol{f} - Q_h \boldsymbol{f}\|_{0,T}^2 \right)^{1/2}.$$

The same statement holds true for η_{DA} *when* $\mathcal{T}_h$ *is composed of triangles and/or rectangles.*

Proof. The upper bound for η_C can be obtained from (12) by summing (14) over $T \in \mathcal{T}_h$ and using the continuity condition (EQ1); see, e.g., [25,20,14]. Therefore we focus on the upper bounds for η_{SR} and η_{DA}.

Using $\boldsymbol{g}_T = \boldsymbol{\sigma}_h \boldsymbol{n}_T|_{\partial T}$ and (8), it follows from (14) that

$$\begin{aligned} A_T(\boldsymbol{\psi}_T, \boldsymbol{v}) &= (\boldsymbol{\sigma}_h - \mu \nabla \boldsymbol{u}_h - (\lambda+\mu) P_h \operatorname{div} \boldsymbol{u}_h \boldsymbol{I}, \nabla \boldsymbol{v})_T + (\boldsymbol{f} + \mathbf{div}\, \boldsymbol{\sigma}_h, \boldsymbol{v})_T \\ &= (\boldsymbol{\sigma}_h - \mu \nabla \boldsymbol{u}_h - (\lambda+\mu) P_h \operatorname{div} \boldsymbol{u}_h \boldsymbol{I}, \nabla \boldsymbol{v})_T + (\boldsymbol{f} - Q_h \boldsymbol{f}, \boldsymbol{v} - P_h \boldsymbol{v})_T, \end{aligned}$$

yielding

$$A_T(\boldsymbol{\psi}_T, \boldsymbol{v}) \le (\eta_{SR,T} + C\mu^{-1/2} h_T \|\boldsymbol{f} - Q_h \boldsymbol{f}\|_{0,T}) \, \mu^{1/2} \|\nabla \boldsymbol{v}\|_{0,T}. \tag{16}$$

When T is a triangle or a rectangle, we combine the explicit formula (9) for $\boldsymbol{\sigma}_h$ with the identity

$$\int_T (\boldsymbol{f} + \mu\Delta\boldsymbol{u}_h)\phi_E^{(T)}\,\mathrm{d}\boldsymbol{x} = \int_T (\boldsymbol{f} - P_h\boldsymbol{f})\phi_E^{(T)}\,\mathrm{d}\boldsymbol{x} + (P_h\boldsymbol{f} + \mu\Delta\boldsymbol{u}_h)\int_T \phi_E^{(T)}\,\mathrm{d}\boldsymbol{x}$$

to obtain (see Remark 2)

$$\boldsymbol{\sigma}_h - \mu\nabla\boldsymbol{u}_h - (\lambda+\mu)P_h\,\mathrm{div}\,\boldsymbol{u}_h\boldsymbol{I} = -\frac{1}{2}(P_h\boldsymbol{f} + \mu\Delta\boldsymbol{u}_h)\otimes(\boldsymbol{x} - \boldsymbol{x}_T) + \boldsymbol{\delta}_T,$$

where

$$\boldsymbol{\delta}_T := -\sum_{E\in\mathcal{E}_T}\left(\int_T (\boldsymbol{f} - P_h\boldsymbol{f})\phi_E^{(T)}\,\mathrm{d}\boldsymbol{x}\right)\otimes\boldsymbol{\theta}_E^{(T)}.$$

By means of the estimates (which can be proved by the scaling argument)

$$\|\phi_E^{(T)}\|_{0,T} \le Ch_T, \qquad \|\boldsymbol{\theta}_E^{(T)}\|_{0,T} \le C,$$

the L^2 norm of $\boldsymbol{\delta}_T$ is bounded by

$$\|\boldsymbol{\delta}_T\|_{0,T} \le \sum_{E\in\mathcal{E}_T}\|\boldsymbol{f} - P_h\boldsymbol{f}\|_{0,T}\|\phi_E^{(T)}\|_{0,T}\|\boldsymbol{\theta}_E^{(T)}\|_{0,T} \le Ch_T\|\boldsymbol{f} - P_h\boldsymbol{f}\|_{0,T}.$$

This again yields (16) now for $\eta_{\mathrm{DA},T}$, noting that $Q_h\boldsymbol{f}|_T = P_h\boldsymbol{f}|_T$. The proof is completed by summing (16) over $T \in \mathcal{T}_h$, applying the Cauchy–Schwarz inequality and then taking $\boldsymbol{v}|_T = \boldsymbol{\psi}_T$. □

Remark 5. Let us see how much η_C can be better than η_{SR} and η_{DA}. Taking $\boldsymbol{v} = \boldsymbol{\psi}_T$ in (16), we obtain

$$|||\boldsymbol{\psi}_T|||_T \le \eta_{SR,T}\frac{\mu^{1/2}\|\nabla\boldsymbol{\psi}_T\|_{0,T}}{|||\boldsymbol{\psi}_T|||_T} + C\mu^{-1/2}h_T\|\boldsymbol{f} - Q_h\boldsymbol{f}\|_{0,T}.$$

This implies that η_C is strictly less than η_{SR} and η_{DA} up to the data oscillation of $\boldsymbol{f}$, unless $\mathrm{div}\,\boldsymbol{\psi}_T \equiv 0$ for every $T \in \mathcal{T}_h$.

Now we are in a position to establish the efficiency of our error estimators. The standard local interpolant $\Pi_T : H^1(T) \to \mathbb{NC}(T)$ is defined by

$$\int_E \Pi_T v\,\mathrm{d}s = \int_E v\,\mathrm{d}s \quad \forall E \in \mathcal{E}_T.$$

For vector-valued functions, Π_T is applied componentwise. The following properties of Π_T are useful in the proof of the subsequent theorem:

$$\int_T \mathrm{div}(\boldsymbol{v} - \Pi_T\boldsymbol{v})\,\mathrm{d}\boldsymbol{x} = 0, \tag{17}$$

$$\|\boldsymbol{v} - \Pi_T\boldsymbol{v}\|_{0,T} \le Ch_T\|\nabla\boldsymbol{v}\|_{0,T}. \tag{18}$$

The global interpolant Π_h is defined in the usual way

$$(\Pi_h\boldsymbol{v})|_T = \Pi_T(\boldsymbol{v}|_T) \quad \forall T \in \mathcal{T}_h.$$

It is easy to check that Π_h maps $\boldsymbol{H}_0^1(\Omega)$ onto $\mathcal{V}_{h,0}\times\mathcal{V}_{h,0}$.

Theorem 5. *Suppose that $\mathcal{T}_h$ consists of triangles and/or rectangles and that every element $T \in \mathcal{T}_h$ has at least two adjacent edges in $\mathcal{E}_\Omega$. Then we have*

$$\eta_C \le C(|||\boldsymbol{u} - \boldsymbol{\xi}||| + \mu^{-1/2}\mathrm{osc}(\boldsymbol{f}, \mathcal{T}_h)).$$

The same statement holds true as well for η_{SR} and η_{DA}.

Proof. By Theorem 4 and the proof therein, it suffices to deal with η_{DA} only. For $\boldsymbol{v} \in \boldsymbol{H}_0^1(\Omega)$, we obtain $P_h\,\mathrm{div}_h(\boldsymbol{v} - \Pi_h\boldsymbol{v}) = 0$ by (17), and thus

$$\begin{aligned} A(\boldsymbol{u} - \boldsymbol{\xi}, \boldsymbol{v}) &= (\boldsymbol{f}, \boldsymbol{v} - \Pi_h\boldsymbol{v})_\Omega - A_h(\boldsymbol{u}_h, \boldsymbol{v} - \Pi_h\boldsymbol{v}) \\ &= (\boldsymbol{f}, \boldsymbol{v} - \Pi_h\boldsymbol{v})_\Omega - \mu(\nabla_h\boldsymbol{u}_h, \nabla_h(\boldsymbol{v} - \Pi_h\boldsymbol{v}))_\Omega \\ &= (\boldsymbol{f} + \mu\Delta_h\boldsymbol{u}_h, \boldsymbol{v} - \Pi_h\boldsymbol{v})_\Omega, \end{aligned}$$

where the last equality follows from

$$\int_T \nabla \boldsymbol{u}_h \cdot \nabla(\boldsymbol{v} - \Pi_h \boldsymbol{v})\,\mathrm{d}\boldsymbol{x} = \int_{\partial T} \frac{\partial \boldsymbol{u}_h}{\partial n_T} \cdot (\boldsymbol{v} - \Pi_h \boldsymbol{v})\,\mathrm{d}s - \int_T \Delta \boldsymbol{u}_h \cdot (\boldsymbol{v} - \Pi_h \boldsymbol{v})\,\mathrm{d}\boldsymbol{x}$$
$$= -\int_T \Delta \boldsymbol{u}_h \cdot (\boldsymbol{v} - \Pi_h \boldsymbol{v})\,\mathrm{d}\boldsymbol{x},$$

since $\frac{\partial \boldsymbol{u}_h}{\partial n_T}|_{\partial T}$ is constant on each edge of T. As a result,

$$(P_h \boldsymbol{f} + \mu \Delta_h \boldsymbol{u}_h, \boldsymbol{v} - \Pi_h \boldsymbol{v})_\Omega = A(\boldsymbol{u} - \boldsymbol{\xi}, \boldsymbol{v}) - (\boldsymbol{f} - P_h \boldsymbol{f}, \boldsymbol{v} - \Pi_h \boldsymbol{v})_\Omega.$$

Now fix an edge $E = \partial T' \cap \partial T''$ and set $\boldsymbol{v} = \operatorname{curl} s$ with $s \in C_0^2(T' \cup T'')$ being compactly supported in $T' \cup T''$. Following closely the argument from the proof of Theorem 2 in [24], one can obtain

$$h_{T'}^2 |(P_h \boldsymbol{f} + \mu \Delta \boldsymbol{u}_h)|_{T'} \cdot \boldsymbol{t}_E| \le C \sum_{T = T', T''} (\mu \|\nabla(\boldsymbol{u} - \boldsymbol{\xi})\|_{0,T} + h_T \|\boldsymbol{f} - P_h \boldsymbol{f}\|_{0,T}),$$

where $\boldsymbol{t}_E$ is the unit tangent vector along E. Further argument in the same proof leads us to the estimate

$$\left(\sum_{T \in \mathcal{T}_h} \mu^{-1} h_T^2 \|P_h \boldsymbol{f} + \mu \Delta \boldsymbol{u}_h\|_{0,T}^2 \right)^{1/2} \le C(\mu^{1/2} \|\nabla(\boldsymbol{u} - \boldsymbol{\xi})\|_{0,\Omega} + \mu^{-1/2} \operatorname{osc}(\boldsymbol{f}, \mathcal{T}_h)),$$

which obviously proves a lower bound for η_{DA}. □

5.2. Nonconforming error estimator

Any choice of $\widetilde{\boldsymbol{u}}_h \in \boldsymbol{H}^1(\Omega; \boldsymbol{u}_D)$ in (13) leads to a computable nonconforming error estimator

$$\eta_{NC} = \mu^{1/2} \left(\|\nabla_h(\widetilde{\boldsymbol{u}}_h - \boldsymbol{u}_h)\|_{0,\Omega} + \frac{1}{m} \|\operatorname{div} \widetilde{\boldsymbol{u}}_h - P_h \operatorname{div}_h \boldsymbol{u}_h\|_{0,\Omega} \right), \tag{19}$$

but for the sake of efficiency, we have to take $\widetilde{\boldsymbol{u}}_h$ as close to $\boldsymbol{u}_h$ as possible at smallest cost. A common choice is to construct a continuous piecewise (bi)quadratic function by averaging $\boldsymbol{u}_h$ at interior Lagrange nodes (excluding hanging nodes) and interpolating $\boldsymbol{u}_D$ at boundary Lagrange nodes.

Remark 6. The estimator (19) is equivalent to the one given in [16], since

$$\|\nabla_h(\widetilde{\boldsymbol{u}}_h - \boldsymbol{u}_h)\|_{0,\Omega} \le C \left(\sum_{E \in \mathcal{E}'_\Omega} h_E^{-1} \|[\![\boldsymbol{u}_h]\!]\|_{0,E}^2 + \sum_{E \in \mathcal{E}_\Gamma} h_E^{-1} \|\boldsymbol{u}_D - \boldsymbol{u}_h\|_{0,E}^2 \right)^{1/2} + C \operatorname{osc}(\boldsymbol{u}_D, \mathcal{E}_\Gamma), \tag{20}$$

where the extra term $\operatorname{osc}(\boldsymbol{u}_D, \mathcal{E}_\Gamma)$ is the data oscillation of $\boldsymbol{u}_D$ defined by

$$\operatorname{osc}(\boldsymbol{u}_D, \mathcal{E}_\Gamma) := \left(\sum_{E \in \mathcal{E}_\Gamma} h_E |\boldsymbol{u}_D - \widetilde{\boldsymbol{u}}_D|_{1,E}^2 \right)^{1/2}.$$

Recall that $\mathcal{E}'_\Omega$ is the set of all truly regular edges and irregular edges. The inequality (20) can be deduced by following the proof of Theorem 2.3 in [33] which considers the homogeneous case $\boldsymbol{u}_D = 0$ (see also [22]).

Although we have $\widetilde{\boldsymbol{u}}_h|_\Gamma = \widetilde{\boldsymbol{u}}_D$, where $\widetilde{\boldsymbol{u}}_D$ is the continuous piecewise quadratic Lagrange interpolant of $\boldsymbol{u}_D$ and thus $\widetilde{\boldsymbol{u}}_h \notin \boldsymbol{H}^1(\Omega; \boldsymbol{u}_D)$ in general, this can only result in a higher order perturbation if $\boldsymbol{u}_D$ is piecewise smooth (cf. [16,22,33]).

Theorem 6. *Let η_{NC} be defined by (19). Then we have*

$$E_h(\boldsymbol{\xi}, \boldsymbol{u}_h) \le \eta_{NC} + C\mu^{1/2} \operatorname{osc}(\boldsymbol{u}_D, \mathcal{E}_\Gamma).$$

Furthermore, the following lower bound holds true

$$\eta_{NC} \le C \left(E_h(\boldsymbol{\xi}, \boldsymbol{u}_h) + \mu^{1/2} \operatorname{osc}(\boldsymbol{u}_D, \mathcal{E}_\Gamma) \right),$$

provided that all triangular elements of $\mathcal{T}_h$ contain no hanging nodes.

Proof. Since the upper bound is discussed in the aforementioned references, we give a proof for the lower bound only. First observe that

$$\begin{aligned}\eta_{NC} &\le \mu^{1/2}\|\nabla_h(\widetilde{\boldsymbol{u}}_h-\boldsymbol{u}_h)\|_{0,\Omega}+\frac{\mu^{1/2}}{m}\|\operatorname{div}_h(\widetilde{\boldsymbol{u}}_h-\boldsymbol{u}_h)\|_{0,\Omega}+\frac{\mu^{1/2}}{m}\|\operatorname{div}_h(\boldsymbol{u}_h-\boldsymbol{\xi})\|_{0,\Omega}+\frac{\mu^{1/2}}{m}\|\operatorname{div}\boldsymbol{\xi}-P_h\operatorname{div}_h\boldsymbol{u}_h\|_{0,\Omega}\\ &\le \left(1+\frac{\sqrt{2}}{m}\right)\mu^{1/2}\|\nabla_h(\widetilde{\boldsymbol{u}}_h-\boldsymbol{u}_h)\|_{0,\Omega}+\frac{\sqrt{2}\,\mu^{1/2}}{m}\|\nabla_h(\boldsymbol{\xi}-\boldsymbol{u}_h)\|_{0,\Omega}+\frac{(\lambda+\mu)^{1/2}}{m}\|\operatorname{div}\boldsymbol{\xi}-P_h\operatorname{div}_h\boldsymbol{u}_h\|_{0,\Omega}\\ &\le C\mu^{1/2}\left(\sum_{E\in\mathcal{E}'_\Omega}h_E^{-1}\|[\![\boldsymbol{u}_h]\!]\|_{0,E}^2+\sum_{E\in\mathcal{E}_\Gamma}h_E^{-1}\|\boldsymbol{u}_D-\boldsymbol{u}_h\|_{0,E}^2\right)^{1/2}+C\left(E_h(\boldsymbol{\xi},\boldsymbol{u}_h)+\mu^{1/2}\operatorname{osc}(\boldsymbol{u}_D,\mathcal{E}_\Gamma)\right),\end{aligned}$$

where (20) was used in the last inequality. Hence it suffices to show that

$$\sum_{E\in\mathcal{E}'_\Omega}h_E^{-1}\|[\![\boldsymbol{u}_h]\!]\|_{0,E}^2+\sum_{E\in\mathcal{E}_\Gamma}h_E^{-1}\|\boldsymbol{u}_D-\boldsymbol{u}_h\|_{0,E}^2\le\|\nabla_h(\boldsymbol{\xi}-\boldsymbol{u}_h)\|_{0,\Omega}^2$$

which is well established if there are no hanging nodes, i.e., $\mathcal{E}'_\Omega$ contains no irregular edges. When there is an irregular edge $E=E_1\cup E_2$ as depicted in Fig. 1, we get

$$\begin{aligned}h_E^{-1}\|[\![\boldsymbol{u}_h]\!]\|_{0,E}^2 &\le Ch_E^{-1}\left\|(\boldsymbol{\xi}-\boldsymbol{u}_h)|_T-\frac{1}{|E|}\int_E(\boldsymbol{\xi}-\boldsymbol{u}_h)|_T\,\mathrm{d}s\right\|_{0,E}^2+C\sum_{i=1,2}h_{E_i}^{-1}\left\|(\boldsymbol{\xi}-\boldsymbol{u}_h)|_{T_i}-\frac{1}{|E|}\int_E(\boldsymbol{\xi}-\boldsymbol{u}_h)|_{T_1\cup T_2}\,\mathrm{d}s\right\|_{0,E_i}^2\\ &:= C(J_1+J_2).\end{aligned}$$

The first term J_1 is estimated in a standard way

$$J_1\le C\|\nabla(\boldsymbol{\xi}-\boldsymbol{u}_h)\|_{0,T}^2.$$

For the second term J_2, we get for any constant c on $T_1\cup T_2$,

$$\begin{aligned}J_2 &= \sum_{i=1,2}h_{E_i}^{-1}\left\|(\boldsymbol{\xi}-\boldsymbol{u}_h-c)|_{T_i}-\frac{1}{|E|}\int_{E_1\cup E_2}(\boldsymbol{\xi}-\boldsymbol{u}_h-c)|_{T_1\cup T_2}\,\mathrm{d}s\right\|_{0,E_i}^2\\ &\le C\sum_{i=1,2}h_{E_i}^{-1}\left(\|(\boldsymbol{\xi}-\boldsymbol{u}_h-c)|_{T_i}\|_{0,E_i}^2+\frac{|E_i|}{|E|^2}\sum_{j=1,2}\left|\int_{E_j}(\boldsymbol{\xi}-\boldsymbol{u}_h-c)|_{T_j}\,\mathrm{d}s\right|^2\right)\\ &\le C\sum_{i=1,2}h_{E_i}^{-1}\left\|(\boldsymbol{\xi}-\boldsymbol{u}_h-c)|_{T_i}\right\|_{0,E_i}^2,\end{aligned}$$

and thus it follows by the trace inequality

$$J_2\le Ch_E^{-2}\|\boldsymbol{\xi}-\boldsymbol{u}_h-c\|_{0,T_1\cup T_2}^2+C\|\nabla_h(\boldsymbol{\xi}-\boldsymbol{u}_h)\|_{0,T_1\cup T_2}^2.$$

Now choosing c to be the integral average of $\boldsymbol{\xi}-\boldsymbol{u}_h$ over $T_1\cup T_2$ and applying the Poincaré inequality [34], we finally obtain

$$h_E^{-1}\|[\![\boldsymbol{u}_h]\!]\|_{0,E}^2\le C\|\nabla_h(\boldsymbol{\xi}-\boldsymbol{u}_h)\|_{0,T\cup T_1\cup T_2}^2.$$

This completes the proof. □

Remark 7. Without the inf–sup condition (11), the estimate (13) would be replaced by

$$E_h(\boldsymbol{\xi},\boldsymbol{u}_h)=\inf_{\boldsymbol{\chi}\in\boldsymbol{H}^1(\Omega;\boldsymbol{u}_D)}E_h(\boldsymbol{\chi},\boldsymbol{u}_h),$$

leading to the nonconforming estimator simply based on the energy norm

$$\eta_{EN}:=E_h(\widetilde{\boldsymbol{u}}_h,\boldsymbol{u}_h).$$

It is obvious that our estimator (19) produces a sharper upper bound than this one as $\lambda\to\infty$. Indeed, numerical experiments reported in the next section reveal that the estimator η_{EN} produces very poor results for large values of λ. This is due to the difficulty of constructing a continuous piecewise polynomial function $\widetilde{\boldsymbol{u}}_h$ in such a way that $(\lambda+\mu)\|\operatorname{div}\widetilde{\boldsymbol{u}}_h-P_h\operatorname{div}_h\boldsymbol{u}_h\|_{0,\Omega}^2$ is bounded as $\lambda\to\infty$.

Computation of η_{NC} or its upper bound requires a precise estimate of the inf–sup constant m or its lower bound. The following theorem provides a lower bound of m for star-shaped domains by following the argument in [35] which relies on Friedrichs' inequality [36]: there exists a constant $\Gamma>0$ depending only on the shape of Ω such that

$$\int_\Omega u^2\,\mathrm{d}\boldsymbol{x}\le\Gamma\int_\Omega v^2\,\mathrm{d}\boldsymbol{x}$$

for all $f=u+\mathrm{i}v$ analytic in Ω with $\int_\Omega u\,\mathrm{d}\boldsymbol{x}=0$.

Theorem 7. *If Ω is star-shaped with respect to the origin, then*

$$m \geq \min_{\boldsymbol{x}\in\partial\Omega} \sqrt{\frac{1-\cos\theta(\boldsymbol{x})}{2}} = \min_{\boldsymbol{x}\in\partial\Omega} \sin\frac{\theta(\boldsymbol{x})}{2},$$

where $0 \leq \theta(\boldsymbol{x}) \leq \frac{\pi}{2}$ is the angle between the radial line from the origin to $\boldsymbol{x} \in \partial\Omega$ and the tangent vector at $\boldsymbol{x}$. If Ω is a polygonal domain, the minimum can occur only at vertices of Ω.

Proof. We combine the equality $m = (1+\Gamma)^{-1/2}$ proved in [35] with the following upper bound for Γ derived in [37]

$$\Gamma \leq \max_{\boldsymbol{x}\in\partial\Omega} \left(\frac{1+\sqrt{1-n_r(\boldsymbol{x})^2}}{n_r(\boldsymbol{x})} \right)^2,$$

where $n_r(\boldsymbol{x})$ is the radial component of the outward unit normal vector at $\boldsymbol{x} \in \partial\Omega$. Since we have $n_r(\boldsymbol{x}) = \sin\theta(\boldsymbol{x})$, it follows that

$$\Gamma \leq \max_{\boldsymbol{x}\in\partial\Omega} \left(\frac{1+\cos\theta(\boldsymbol{x})}{\sin\theta(\boldsymbol{x})} \right)^2 = \max_{\boldsymbol{x}\in\partial\Omega} \frac{1+\cos\theta(\boldsymbol{x})}{1-\cos\theta(\boldsymbol{x})},$$

which gives the desired lower bound for m. Finally, we observe that the minimum occurs at one of the endpoints if $\boldsymbol{x}$ moves over a line segment. □

By means of this theorem and the lower bound for Γ from [36], it was shown in [35] that $0.3826 < m < 0.4263$ for the square and $0.1601 < m < 0.4263$ for the L-shape domain. The estimate for the L-shape domain seems rather pessimistic as the numerical value $m_h = 0.3101$ was obtained in [35] by solving the discrete eigenvalue problem for the Stokes equation discretized by the $P1$ nonconforming finite element method on the uniform triangular grid with the grid size $h = \frac{1}{32}$.

Remark 8. The abstract upper bounds for η_C, η_{SR} and η_{NC} given in Lemma 3, Theorems 4 and 6 apply for general quadrilateral meshes. The same is true for the construction of $\boldsymbol{g}_T$, $\boldsymbol{\sigma}_h$ and $\widetilde{\boldsymbol{u}}_h$, implying that both the pairs η_C–η_{NC} and η_{SR}–η_{NC} are reliable for general quadrilateral meshes. The restrictive assumption of rectangular elements is made when the simpler conforming estimator η_{DA} is derived in Theorem 4 through the explicit formula (9) of $\boldsymbol{\sigma}_h$ and then the lower bound for the conforming estimator is established in Theorem 5.

6. Numerical experiments

In this section numerical results are presented to demonstrate the robustness and accuracy of a posteriori error estimators proposed in the previous section. When computing η_C, we solve the local Neumann problem (14) in $(\mathbb{P}_2(T))^2$. The nonconforming estimator η_{NC} is computed by

$$\eta_{NC} = \mu^{1/2} \left(\|\nabla_h(\widetilde{\boldsymbol{u}}_h - \boldsymbol{u}_h)\|_{0,\Omega}^2 + \frac{1}{m^2} \|\operatorname{div}\widetilde{\boldsymbol{u}}_h - P_h \operatorname{div}_h \boldsymbol{u}_h\|_{0,\Omega}^2 \right)^{1/2}$$

so that it may be represented as the square root of the l^2 sum $\sum_{T\in\mathcal{T}_h} \eta_{NC,T}^2$. This is equivalent to, but slightly smaller than (19).

6.1. Example 1

The domain is taken to be the unit square $\Omega = (0,1)^2$, and the exact solution $\boldsymbol{u} = (u_1, u_2)$ is given by

$$u_1(x,y) = \cos(2\pi x)\sin(2\pi y), \qquad u_2(x,y) = -u_1(y,x)$$

with the corresponding data $\boldsymbol{f}$ and $\boldsymbol{u}_D$. The Lamé constants are set to be $\mu = 1$ and $\lambda = 10, 10^3$, and the theoretical lower bound $m = 0.38$ is used for the inf–sup constant. A sequence of meshes is generated by uniform mesh refinement starting with the 2×2 triangular or quadrilateral mesh shown in Fig. 2. Since $\boldsymbol{u}$ is smooth, we do not consider adaptive mesh refinement.

In Tables 1 and 2 we compare the implicit estimator η_C and the explicit one η_{DA} or η_{SR} as well as the two nonconforming estimators η_{NC} and η_{EN} for the value of $\lambda = 10^3$, along with the effectivity indices defined by

$$\theta_{NC} := \frac{(\eta_C^2 + \eta_{NC}^2)^{1/2}}{E_h(\boldsymbol{u}, \boldsymbol{u}_h)}, \qquad \theta_{EN} := \frac{(\eta_C^2 + \eta_{EN}^2)^{1/2}}{E_h(\boldsymbol{u}, \boldsymbol{u}_h)}.$$

As explained in Remark 5, η_C yields better results than the explicit estimator, by 20% in this particular example. A dramatic improvement is observed for η_{NC} and θ_{NC} which are found to be ten times smaller than η_{EN} and θ_{EN}, respectively. This is also clearly seen in Figs. 3–4, where true errors in the energy norm and two error estimators with the combinations η_C–η_{NC} and η_C–η_{EN} are plotted versus the number of degrees of freedom for triangular meshes. In agreement with the theory, the former combination gives uniform bounds in λ, whereas the latter one gets worse as λ grows. Quadrilateral elements exhibit very similar behaviors, and so we omit the figures.

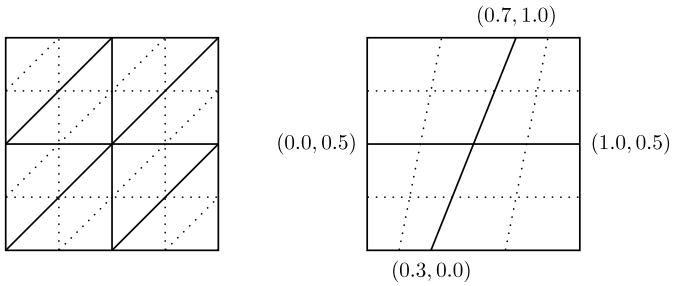

Fig. 2. Initial triangular and quadrilateral meshes for Example 1. Uniform mesh refinement is indicated by dotted lines.

Table 1
Comparison of error estimators (η_C vs. η_{DA} and η_{NC} vs. η_{EN}) and effectivity indices (θ_{NC} vs. θ_{EN}) for Example 1 with $\lambda = 10^3$ on triangular meshes.

DOFs	η_C	η_{DA}	η_{NC}	η_{EN}	θ_{NC}	θ_{EN}
416	9.745e−1	1.124e+0	2.889e+0	2.978e+1	1.745	17.042
1600	4.832e−1	5.766e−1	1.689e+0	1.818e+1	1.974	20.422
6272	2.410e−1	2.902e−1	8.940e−1	9.734e+0	2.070	21.765
24832	1.204e−1	1.453e−1	4.561e−1	4.986e+0	2.106	22.266
98816	6.021e−2	7.269e−2	2.298e−1	2.516e+0	2.121	22.467
394240	3.010e−2	3.635e−2	1.153e−1	1.263e+0	2.127	22.555

Table 2
Comparison of error estimators (η_C vs. η_{SR} and η_{NC} vs. η_{EN}) and effectivity indices (θ_{NC} vs. θ_{EN}) for Example 1 with $\lambda = 10^3$ on quadrilateral meshes.

DOFs	η_C	η_{SR}	η_{NC}	η_{EN}	θ_{NC}	θ_{EN}
288	1.254e+0	1.621e+0	3.142e+0	3.251e+1	1.571	15.105
1088	6.254e−1	7.754e−1	1.660e+0	1.756e+1	1.675	16.596
4224	3.122e−1	3.822e−1	8.446e−1	9.010e+0	1.708	17.102
16640	1.560e−1	1.904e−1	4.251e−1	4.549e+0	1.720	17.288
66048	7.801e−2	9.511e−2	2.131e−1	2.284e+0	1.725	17.363
263168	3.900e−2	4.754e−2	1.067e−1	1.144e+0	1.727	17.397

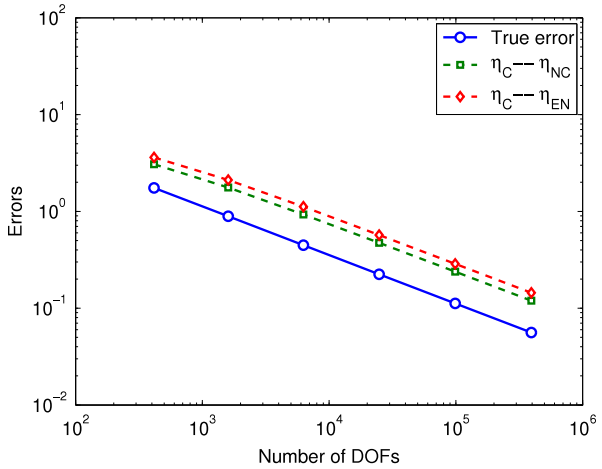

Fig. 3. True error and two error estimators for Example 1 with $\lambda = 10$ on triangular meshes.

6.2. Example 2

The second example is taken from [9–11]. The domain is shown in Fig. 5 which is obtained via clockwise rotation of the L-shaped domain $(-1, 1)^2 \setminus (-1, 0)^2$ by $\pi/4$. The exact solution $\boldsymbol{u}$ given in polar coordinates (r, θ), $-\pi < \theta \leq \pi$, centered at the origin is

$$u_r(r, \theta) = \frac{r^\alpha}{2\mu}(-(\alpha + 1)\cos((\alpha + 1)\theta) + (C_2 - \alpha - 1)C_1 \cos((\alpha - 1)\theta)),$$

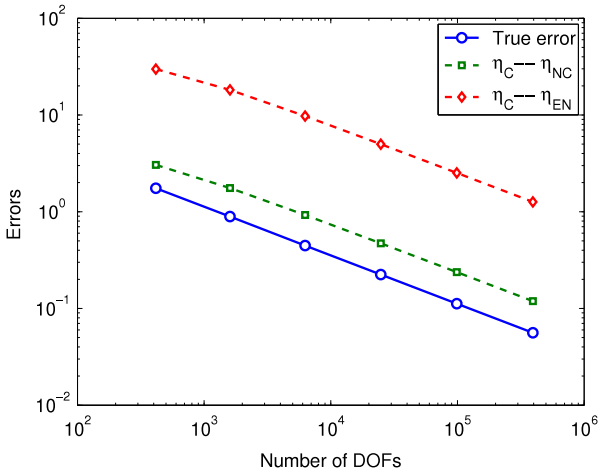

Fig. 4. True error and two error estimators for Example 1 with $\lambda = 10^3$ on triangular meshes.

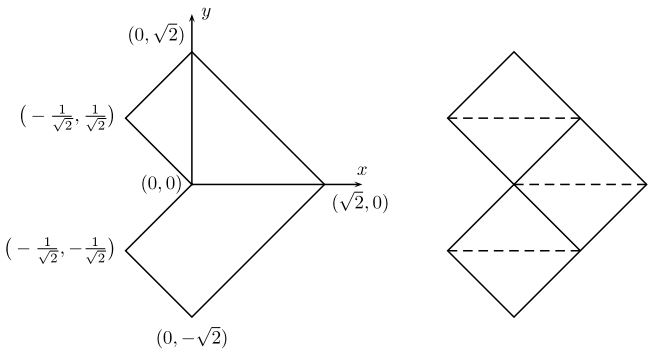

Fig. 5. Domain geometry and initial meshes for Example 2. The quadrilateral mesh consists of three rotated squares, and the triangular mesh is obtained by further division (dashed lines).

$$u_\theta(r,\theta) = \frac{r^\alpha}{2\mu}((\alpha+1)\sin((\alpha+1)\theta) + (C_2+\alpha-1)C_1\sin((\alpha-1)\theta)),$$

where $\alpha = 0.54448373\cdots$ is the positive solution of $\alpha\sin\left(\frac{3\pi}{2}\right) + \sin\left(\frac{3\pi}{2}\alpha\right) = 0$, and

$$C_1 = -\frac{\cos\left((\alpha+1)\frac{3\pi}{4}\right)}{\cos\left((\alpha-1)\frac{3\pi}{4}\right)}, \qquad C_2 = \frac{2(\lambda+2\mu)}{\lambda+\mu}.$$

This solution has a singularity near the re-entrant corner at the origin.

Since $\boldsymbol{f} = (0, 0)$, all conforming estimators vanish if the mesh is composed of triangles or rotated squares, in which case the total error estimator $\eta = \left(\sum_{T\in\mathcal{T}_h}\eta_T^2\right)^{1/2}$ only consists of the nonconforming contribution

$$\eta_T^2 = \mu\left(\|\nabla(\widetilde{\boldsymbol{u}}_h - \boldsymbol{u}_h)\|_{0,T}^2 + \frac{1}{m^2}\|\operatorname{div}\widetilde{\boldsymbol{u}}_h - P_h\operatorname{div}_h\boldsymbol{u}_h\|_{0,T}^2\right).$$

The numerical value $m = 0.3$ is chosen for the inf–sup constant (which is invariant under rotation). Based on this error estimator, we perform adaptive mesh refinement starting with the meshes shown in Fig. 5 and following the simple maximum strategy in which an element T is marked for refinement if

$$\eta_T \geq 0.5\max_{T'\in\mathcal{T}_h}\eta_{T'}.$$

Further elements are marked to avoid hanging nodes for triangular meshes and to keep the 1-irregular rule plus the "full neighbor rule" for quadrilateral meshes. The "full neighbor rule" means that an element should be refined if all its neighbors have been refined.

Table 3
Effectivity indices for Example 2 on uniform triangular and quadrilateral meshes.

Level	Triangular		Quadrilateral	
	$\lambda = 10$	$\lambda = 10^3$	$\lambda = 10$	$\lambda = 10^3$
0	3.176	3.127	2.757	2.669
1	3.059	2.992	2.716	2.603
2	3.056	2.981	2.752	2.643
3	3.077	3.008	2.770	2.665
4	3.084	3.019	2.775	2.674
5	3.086	3.022	2.779	2.677
6	3.086	3.023	2.780	2.678
7	3.087	3.024	2.780	2.678

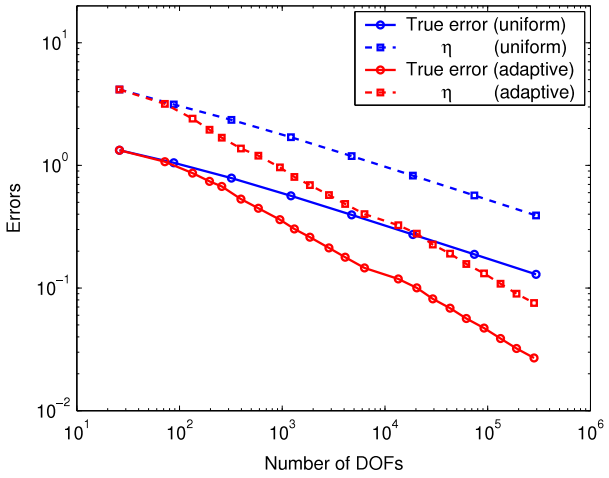

Fig. 6. True errors and error estimators for Example 2 with $\lambda = 10^3$ on triangular meshes. The order of convergence is $O(N^{-0.25})$ for uniform meshes and $O(N^{-0.45})$ for adaptive meshes.

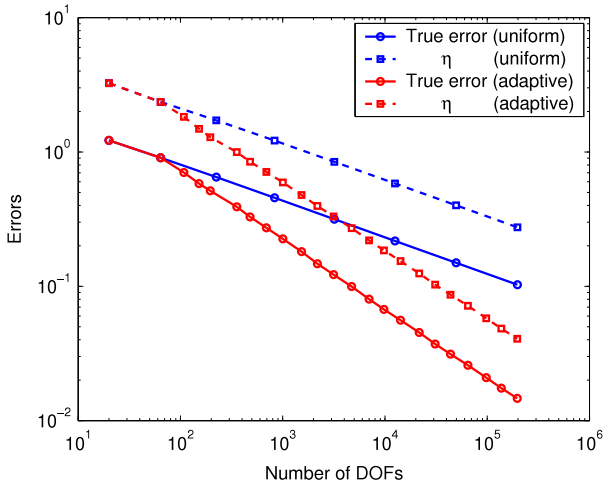

Fig. 7. True errors and error estimators for Example 2 with $\lambda = 10^3$ on quadrilateral meshes. The order of convergence is $O(N^{-0.27})$ for uniform meshes and $O(N^{-0.50})$ for adaptive meshes.

We report the results for $\mu = 1$ and $\lambda = 10, 10^3$. In Table 3 the effectivity indices are displayed which remain close to a relatively small value in all cases. For $\lambda = 10^3$, reduction of true errors and error estimators are plotted in Fig. 6 for triangular meshes and in Fig. 7 for quadrilateral meshes. It is observed that the order of convergence is roughly the theoretically predicted value, $\gamma \approx 0.27$, for uniform mesh refinement, whereas adaptive mesh refinement almost achieves the optimal order of convergence, $\gamma \approx 0.5$. Adapted triangular and quadrilateral meshes after 8 and 16 refinements are also shown in Fig. 8. As expected, the mesh refinement is highly concentrated around the re-entrant corner where $\boldsymbol{u}$ is very singular.

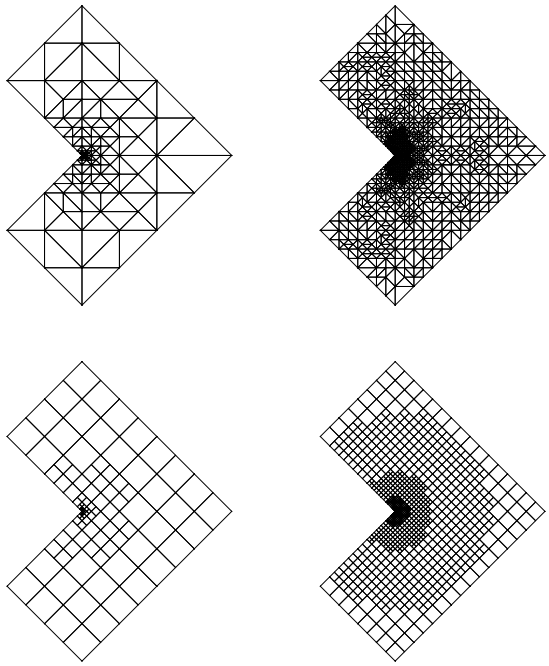

Fig. 8. Adapted triangular and quadrilateral meshes generated after 6 and 12 refinements for Example 2 with $\lambda = 10^3$.

References

[1] S.C. Brenner, L.R. Scott, The Mathematical Theory of Finite Element Methods, Springer-Verlag, New York, 1994.
[2] S.C. Brenner, L.-Y. Sung, Linear finite element methods for planar linear elasticity, Math. Comp. 59 (200) (1992) 321–338.
[3] R.S. Falk, Nonconforming finite element methods for the equations of linear elasticity, Math. Comp. 57 (196) (1991) 529–550.
[4] R. Kouhia, R. Stenberg, A linear nonconforming finite element method for nearly incompressible elasticity and Stokes flow, Comput. Methods Appl. Mech. Engrg. 124 (3) (1995) 195–212.
[5] C. Lee, J. Lee, D. Sheen, A locking-free nonconforming finite element method for planar linear elasticity, Adv. Comput. Math. 19 (1–3) (2003) 277–291.
[6] Z. Zhang, Analysis of some quadrilateral nonconforming elements for incompressible elasticity, SIAM J. Numer. Anal. 34 (2) (1997) 640–663.
[7] M. Ainsworth, J.T. Oden, A Posteriori Error Estimation in Finite Element Analysis, John Wiley & Sons, 2000.
[8] R. Verfürth, A Review of a Posteriori Error Estimation and Adaptive Mesh-Refinement Techniques, Wiley, Teubner, 1996.
[9] C. Carstensen, S.A. Funken, Averaging technique for FE—a posteriori error control in elasticity. I. Conforming FEM, Comput. Methods Appl. Mech. Engrg. 190 (18–19) (2001) 2483–2498.
[10] C. Carstensen, S.A. Funken, Averaging technique for FE—a posteriori error control in elasticity. II. λ-independent estimates, Comput. Methods Appl. Mech. Engrg. 190 (35–36) (2001) 4663–4675.
[11] C. Carstensen, S.A. Funken, Averaging technique for a posteriori error control in elasticity. III. Locking-free nonconforming FEM, Comput. Methods Appl. Mech. Engrg. 191 (8–10) (2001) 861–877.
[12] U. Brink, E. Stein, A posteriori error estimation in large-strain elasticity using equilibrated local Neumann problems, Comput. Methods Appl. Mech. Engrg. 161 (1–2) (1998) 77–101.
[13] C. Carstensen, R. Klose, A. Orlando, Reliable and efficient equilibrated a posteriori finite element error control in elastoplasticity and elastoviscoplasticity with hardening, Comput. Methods Appl. Mech. Engrg. 195 (19–22) (2006) 2574–2598.
[14] S. Ohnimus, E. Stein, E. Walhorn, Local error estimates of FEM for displacements and stresses in linear elasticity by solving local Neumann problems, Internat. J. Numer. Methods Engrg. 52 (7) (2001) 727–746.
[15] S. Nicaise, K. Witowski, B. Wohlmuth, An a posteriori error estimator for the Lamé equation based on equilibrated fluxes, IMA J. Numer. Anal. 28 (2) (2008) 331–353.
[16] C. Carstensen, J. Hu, A unifying theory of a posteriori error control for nonconforming finite element methods, Numer. Math. 107 (3) (2007) 473–502.
[17] R. Verfürth, A review of a posteriori error estimation techniques for elasticity problems, Comput. Methods Appl. Mech. Engrg. 176 (1–4) (1999) 419–440.
[18] C. Carstensen, J. Hu, Hanging nodes in the unifying theory of a posteriori finite element error control, J. Comput. Math. 27 (2–3) (2009) 215–236.
[19] Kwang Y. Kim, A posteriori error analysis for locally conservative mixed methods, Math. Comp. 76 (257) (2007) 43–66.
[20] Kwang Y. Kim, A posteriori error estimators for locally conservative methods of nonlinear elliptic problems, Appl. Numer. Math. 57 (9) (2007) 1065–1080.
[21] F. Schieweck, A posteriori error estimates with post-processing for nonconforming finite elements, M2AN Math. Model. Numer. Anal. 36 (3) (2002) 489–503.
[22] C. Carstensen, J. Hu, A. Orlando, Framework for the a posteriori error analysis of nonconforming finite elements, SIAM J. Numer. Anal. 45 (1) (2007) 68–82.
[23] E. Dari, R. Durán, C. Padra, Error estimators for nonconforming finite element approximations of the Stokes problem, Math. Comp. 64 (211) (1995) 1017–1033.
[24] W. Dörfler, M. Ainsworth, Reliable a posteriori error control for nonconforming finite element approximation of Stokes flow, Math. Comp. 74 (252) (2005) 1599–1619.
[25] M. Ainsworth, J.T. Oden, A unified approach to a posteriori error estimation using element residual methods, Numer. Math. 65 (1) (1993) 23–50.
[26] R.E. Bank, A. Weiser, Some a posteriori error estimators for elliptic partial differential equations, Math. Comp. 44 (170) (1985) 283–301.
[27] L.D. Marini, An inexpensive method for the evaluation of the solution of the lowest order Raviart–Thomas mixed method, SIAM J. Numer. Anal. 22 (3) (1985) 493–496.

[28] J. Hu, J.C. Xu, Convergence of adaptive conforming and nonconforming finite element methods for the perturbed Stokes equation, Research Report 73, LMAM and School of Mathematical Sciences, Peking University, 2007.
[29] M. Crouzeix, P.A. Raviart, Conforming and nonconforming finite element methods for solving the stationary Stokes equations, RAIRO 7 (R-3) (1973) 33–75.
[30] R. Rannacher, S. Turek, Simple nonconforming quadrilateral Stokes element, Numer. Methods Partial Differential Equations 8 (2) (1992) 97–111.
[31] P. Ladavèze, E.A.W. Maunder, A general method for recovering equilibrating element tractions, Comput. Methods Appl. Mech. Engrg. 137 (2) (1996) 111–151.
[32] F. Brezzi, M. Fortin, Mixed and Hybrid Finite Element Methods, Springer-Verlag, New York, 1991.
[33] O. Karakashian, F. Pascal, A posteriori error estimates for a discontinuous Galerkin approximation of second-order elliptic problems, SIAM J. Numer. Anal. 41 (6) (2003) 2374–2399.
[34] S.C. Brenner, Poincaré–Friedrichs inequalities for piecewise H^1 functions, SIAM J. Numer. Anal. 41 (1) (2003) 306–324.
[35] G. Stoyan, Towards discrete Velte decompositions and narrow bounds for inf–sup constants, Comput. Math. Appl. 38 (7–8) (1999) 243–261.
[36] K. Friedrichs, On certain inequalities and characteristic value problems for analytic functions and for functions of two variables, Trans. Amer. Math. Soc. 41 (3) (1937) 321–364.
[37] C.O. Horgan, L.E. Payne, On inequalities of Korn, Friedrichs and Babuǩa–Aziz, Arch. Ration. Mech. Anal. 82 (2) (1983) 165–179.